Neural Networks 180 (2024) 106732

Contents lists available at ScienceDirect

Neural Networks

journal homepage: www.elsevier.com/locate/neunet

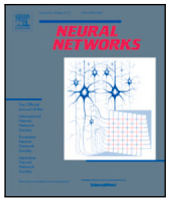

Full Length Article

Coagulo-Net: Enhancing the mathematical modeling of blood coagulation using physics-informed neural networks

Ying Qian [a,1], Ge Zhu [b,1], Zhen Zhang [c,1], Susree Modepalli [d], Yihao Zheng [e], Xiaoning Zheng [f], Galit Frydman [g,h], He Li [a,*]

[a] School of Chemical, Materials and Biomedical Engineering, University of Georgia, Athens, USA
[b] Department of Biomedical Engineering, Worcester Polytechnic Institute, Worcester, USA
[c] Division of Applied Mathematics, Brown University, Providence, RI, USA
[d] School of Medicine, Georgetown University, Washington DC, USA
[e] Department of Mechanical and Material Engineering, Worcester Polytechnic Institute, Worcester, USA
[f] Department of Mathematics, College of Information Science & Technology, Jinan University, Guangzhou, Guangdong, 510632, China
[g] Division of Trauma, Emergency Surgery and Surgical Critical Care at the Massachusetts General Hospital, Boston, MA, USA
[h] Division of Comparative Medicine, Department of Biological Engineering, Massachusetts Institute of Technology, Cambridge, MA, USA

ARTICLE INFO

Dataset link: https://github.com/dpdclub/Coagulo-net.git

Keywords:
Mathematical modeling of blood coagulation
Physics-informed neural network (PINN)
Blood clotting
Neural networks
Thrombosis

ABSTRACT

Blood coagulation, which involves a group of complex biochemical reactions, is a crucial step in hemostasis to stop bleeding at the injury site of a blood vessel. Coagulation abnormalities, such as hypercoagulation and hypocoagulation, could either cause thrombosis or hemorrhage, resulting in severe clinical consequences. Mathematical models of blood coagulation have been widely used to improve the understanding of the pathophysiology of coagulation disorders, guide the design and testing of new anticoagulants or other therapeutic agents, and promote precision medicine. However, estimating the parameters in these coagulation models has been challenging as not all reaction rate constants and new parameters derived from model assumptions are measurable. Although various conventional methods have been employed for parameter estimation for coagulation models, the existing approaches have several shortcomings. Inspired by the physics-informed neural networks, we propose Coagulo-Net, which synergizes the strengths of deep neural networks with the mechanistic understanding of the blood coagulation processes to enhance the mathematical models of the blood coagulation cascade. We assess the performance of the Coagulo-Net using two existing coagulation models with different extents of complexity. Our simulation results illustrate that Coagulo-Net can efficiently infer the unknown model parameters and dynamics of species based on sparse measurement data and data contaminated with noise. In addition, we show that Coagulo-Net can process a mixture of synthetic and experimental data and refine the predictions of existing mathematical models of coagulation. These results demonstrate the promise of Coagulo-Net in enhancing current coagulation models and aiding the creation of novel models for physiological and pathological research. These results showcase the potential of Coagulo-Net to advance computational modeling in the study of blood coagulation, improving both research methodologies and the development of new therapies for treating patients with coagulation disorders.

1. Introduction

The human blood coagulation cascade is a complex biochemical process (Dahlbäck, 2000) with a crucial role in reducing blood loss during vascular damage due to physical injury. The process, known as hemostasis, involves the body stopping blood loss post-injury through enzyme activation that drives the formation of a clot over the wound. The body achieves homeostasis by balancing three critical hemostatic processes: vasodilation, blood coagulation, and clot dissolution. An imbalance in these processes can cause abnormal hemostasis, leading to potentially life-threatening conditions. For instance, a deficiency in coagulation factors, such as in hemophilia (Butenas, van't Veer, & Mann, 1999) or irregular fibrinolysis (Bachman, 1987), can result in rapid blood loss. Conversely, a mutation in coagulation factors, like the Factor V Leiden Mutation, makes the protein more resistant to degradation by the body's natural anticoagulant, protein C. This

* Corresponding author.
E-mail address: he.li3@uga.edu (H. Li).
[1] Equally contributed.

https://doi.org/10.1016/j.neunet.2024.106732
Received 17 April 2024; Received in revised form 30 August 2024; Accepted 10 September 2024
Available online 19 September 2024

resistance allows factor V to stay active, resulting in excessive clotting (thrombosis) (Herrmann et al., 1997; Vandenbroucke et al., 1994). Both hemorrhagic and thrombotic diseases could potentially lead to fatal clinical outcomes (Li, Zhao, Ma, Gao, & Zhao, 2024). Thus, maintaining a balance in hemostatic processes is essential for healthy physiological functioning.

The coagulation cascade is divided into four distinct phases: initiation, amplification, propagation, and stabilization (Furie & Furie, 2008; Hoffman & Monroe III, 2001). The initiation phase begins with tissue factor (TF) expression at the site of vessel damage, leading to the activation of clotting proteins factor IX and X by factor VIIa (Camerer, Huang, & Coughlin, 2000). The TF-VIIa complex, forming at the injury site, links the intrinsic and extrinsic coagulation pathways (Palta, Saroa, & Palta, 2014). This complex's formation can be halted using a TF inhibitor to prevent thrombin generation (Chatterjee, Denney, Jing and Diamond, 2010). During the amplification phase, there is a significant increase in thrombin generation, which, in turn, activates platelets. Thrombin also activates factors VIII and V, which are crucial for forming tenase and prothrombinase complexes on activated platelets. These complexes greatly enhance prothrombin activation. In the propagation phase, these complexes accumulate on platelet surfaces, supporting continuous thrombin generation and fibrin formation at the injury site. Finally, the stabilization phase is marked by the activation of factor XIII, which cross-links fibrin strands into stable fibrin plugs. Additionally, thrombin-activatable fibrinolysis inhibitors (TAFI) are activated, supporting the newly formed fibrin and preventing excessive fibrinolysis.

The area of blood coagulation and hemostasis encompasses a wide range of significant topics, including the kinetics of coagulation factors, the spatial–temporal structure of blood clots, the influence of fluid flow on clotting, system pharmacology modeling of clotting, among others. However, a significant challenge in current research is the dependency on extensive, costly lab experiments. Predicting thrombosis and other thrombotic events in clinical settings is difficult due to the lengthy time required for laboratory testing (Lippi & Favaloro, 2020). This delay in test results poses a challenge in the clinical management of thrombosis. Many researchers are turning to mathematical and computational modeling to overcome this issue. Over the past three decades, mathematical and computational modeling has been increasingly used to gain insights into hemostasis (see reviews Anand, Panteleev, & Ataullakhanov, 2022; Belyaev, Dunster, Gibbins, Panteleev, & Volpert, 2018; Leiderman & Fogelson, 2014; Leiderman, Sindi, Monroe, Fogelson, & Neeves, 2021; Link et al., 2021; Neeves & Leiderman, 2016; Zhu, Modepalli, Anand, & Li, 2023) and offer practical solutions by simulating how the dynamics of the blood coagulation cascade vary under different physiological conditions.

Current mathematical models for simulating hemostasis at the continuum level are categorized into two main types: ordinary differential equation (ODE) models and partial differential equation (PDE) models. ODE models, which are designed to mimic thrombin and fibrin generation assays, operate on the principle that biochemical reactions can be represented as kinetic equations derived from experimental data (Beltrami & Jesty, 1995; Bungay, Gentry, & Gentry, 2003; Chatterjee, Purvis, Brass and Diamond, 2010; Dashkevich et al., 2012; Fogelson & Tania, 2005; Hockin, Jones, Everse, & Mann, 2002; Kuharsky & Fogelson, 2001). These models focus on temporal changes, illustrating how coagulation factor concentrations evolve over time under spatially uniform conditions. They are particularly useful for predicting concentration changes and identifying new reaction mechanisms, especially when there is a discrepancy between model predictions and actual data. In contrast, PDE models are utilized to simulate thrombus growth, taking into account both unstirred systems and blood flow conditions (Bouchnita, 2017; Bouchnita, Terekhov, Nony, Vassilevski, & Volpert, 2020; Bouchnita & Volpert, 2019; Bouchnita, Yadav, Llored, Gurovich, & Volpert, 2023; Leiderman & Fogelson, 2011, 2013; Panteleev et al., 2006; Zarnitsina, Pokhilko, & Ataullakhanov, 1996). These spatio-temporal models are essential for understanding clot growth within blood vessels, as they consider spatial concentration variations and can integrate blood flow velocity, often through a convection term, to provide deeper insights into the clot formation and growth dynamics.

It is noted that not all rate constants involved in the coagulation model can be measured. In addition, when model assumptions and approximations are made, new parameters that are not measurable are sometimes generated. In these cases, model parameters must be assessed based on mostly experimental data. Thus, parameter estimation is crucial in validating existing models and developing accurate and reliable new models for the blood coagulation process. Various methods have been widely used for parameter estimation when building coagulation models, including least squares estimation, maximum likelihood estimation, Bayesian methods, and global optimization techniques. However, these conventional methods have their drawbacks, including being time and labor-intensive, particularly for extensive parameter spaces, functioning only under specific assumptions, and necessitating fine-tuning parameters for optimal algorithm performance. Therefore, it is essential to investigate novel algorithms capable of efficiently estimating unmeasurable model parameters, which will aid in developing computational biology models. Recently, there has been a surge in the use of scientific machine learning models that blend neural networks (NNs) with physics-based modeling. These scientific machine-learning models are particularly effective for training NNs with limited data (Li et al., 2023; Raissi, 2018; Raissi, Perdikaris, & Karniadakis, 2019). Physics-informed neural networks (PINNs) and their emerging extensions have become popular for addressing inverse or complex problems (De Ryck, Jagtap, & Mishra, 2024; Jagtap & Karniadakis, 2020; Jagtap, Kawaguchi, & Em Karniadakis, 2020a; Jagtap, Kawaguchi, & Karniadakis, 2020b; Jagtap, Kharazmi and Karniadakis, 2020; Jagtap, Mao, Adams, & Karniadakis, 2022; Mao, Jagtap, & Karniadakis, 2020; Shukla, Jagtap, Blackshire, Sparkman and Karniadakis, 2021; Shukla, Jagtap and Karniadakis, 2021). They integrate ordinary or partial differential equation models with sparse data sources like measurements or images (Cai et al., 2021; Kissas et al., 2020; Lei, Liu, & Wang, 2022; Nguyen, Dairay, Meunier, & Mougeot, 2022; Ouyang et al., 2023; Sahli Costabal, Yang, Perdikaris, Hurtado, & Kuhl, 2020). PINNs have been successfully used in various applications to deduce unknown parameters in these equation models by optimizing an objective function constrained by both the model and data loss (Cai, Mao, Wang, Yin, & Karniadakis, 2022; Du, Zhu, & Wang, 2022; Jagtap, Kharazmi et al., 2020; Karniadakis et al., 2021; Lorenzo et al., 2022; Ren, Rao, Sun, & Liu, 2022; Yang, Meng, & Karniadakis, 2021; Zhang, Dao, Karniadakis, & Suresh, 2022).

Building on the concept of PINNs (Raissi et al., 2019), we introduce a method to integrate the mathematical models of the blood coagulation cascade into the loss functions of a neural network, which we call Coagulo-Net. As shown in Fig. 1, this approach allows the unknown model parameters to be treated as trainable, determined by minimizing the loss function. Moreover, the enforcement of the equations in the loss function also adds a regularization effect that makes this algorithm robust to noise. Prior work of Yazdani, Lu, Raissi, and Karniadakis (2020) has demonstrated that PINNs enable inference of unknown kinetic rates and missing dynamics of the species in several simple biological ODE models with only partial data. In this work, we will systematically investigate the performance of the Coagulo-Net on learning the unknown model parameters of the coagulation models. The remainder of the paper is organized as follows: In Section 2 (Models and methods), we introduce the structure and each component of Coagulo-Net as well as two mathematical models of blood coagulation we incorporate into the Coagulo-Net. In Section 3 (Results), we demonstrate the effectiveness of Coagulo-Net in inferring unknown parameters from two coagulation models with different levels of complexity. We conclude in Section 4 (Discussion and summary) with an overview of the current study, a summary of the model limitations, and a list of potential future work.

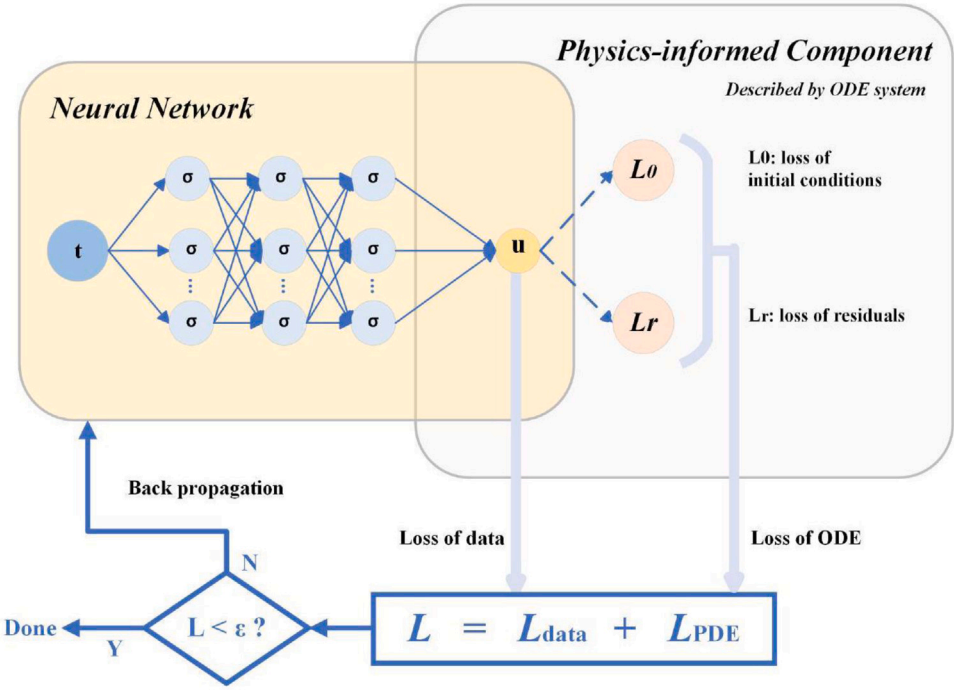

Fig. 1. The structure of Coagulo-Net. Coagulo-Net takes time t as input and output the coagulation factors **u** involved in the coagulation models. The loss function of the Coagulo-Net consists of two parts: data loss and physics-informed loss. Physics-informed loss is composed of loss calculated from initial conditions and residuals of the ODEs.

2. Models and methods

2.1. Two mathematical models of blood coagulation with different levels of complexity

One of the earliest spatial–temporal models for blood coagulation was proposed by Zarnitsina et al. (1996) (hereafter referred to as Zarnitsina's model), and it models the intrinsic pathway. Zarnitsina's model consists of ODEs for eight factors, with tenase and prothrombinase being calculated as "quick" variables (quasi-stationary concentrations) and factor XI being specified as an initial condition. Although Zarnitsina's model does not capture the kinetics of many enzymes, the ODE model can still be used as an effective mathematical model to simulate clotting dynamics under certain conditions. Here, to demonstrate the effectiveness of Coagulo-Net, we will use the homogeneous Zarnitsina's model, which consists of only 8 ODEs. In addition to Zarnitsina's model, we employ another mathematical model developed by Susree and Anand (2017) (hereafter referred to as Susree's model), which consists of ODEs for 34 species to consider more coagulation factors and the role of activated platelets (as a separate species, as well as in binding of tenase/prothrombinase complexes) in clot formation and growth.

The typical form of the ODEs employed in either Zarnitsina's or Susree's models is of the form listed in Eq. (1):

$$\frac{du(t)}{dt} = g(u(t), t). \tag{1}$$

In the above equation, $u(t)$ is the concentration of species u as a function of time t. The detailed mathematical expressions of Zarnitsina's and Susree's models are listed in Appendices A and B, respectively. Numerical computations for the system of differential equations in each model were performed by variable order method (Cash & Karp, 1990) in MATLAB environment (MATLAB 2021b Academic Version). The kinetic constants for each reaction in the models follow the value used in the original work of Susree and Anand (2017) and Zarnitsina et al. (1996), respectively. The model parameters and initial values of each species used for the mathematical model simulations are adopted from the original publication of Susree's model (Susree & Anand, 2017) and Zarnitsina's model (Zarnitsina et al., 1996). The initial values of the coagulation factors and the model parameters for the two models are attached in the Appendix.

2.2. Integrating coagulation models with neural network using Coagulo-Net

As illustrated in Fig. 1, the Coagulo-Net consists of a fully connected neural network made of three hidden layers with 100 neurons in each layer. Coagulo-Net takes time as input and outputs eight state variables in the case of Zarnitsina's model and 34 state variables in the case of Susree's model, corresponding to the coagulation factors involved in the two coagulation models. All the state variables will be used to calculate the loss of data. To facilitate training the Coagulo-net, all the coagulation factors are scaled by their magnitude such that they are varied between 0 and 10. The effect of the coagulation model is incorporated into the training of Coagulo-Net by computing the loss of ODE. The total loss of Coagulo-Net equals the sum of the loss of data and loss of ODE, and it can expressed as

$$\mathcal{L} = w_{data}\mathcal{L}_{data} + w_{ODE}\mathcal{L}_{ODE}, \tag{2}$$

where w_{data} and w_{ODE} are weights that are adjusted to ensure the data loss and ODE loss are on the same scale. The data loss is computed by

$$\mathcal{L}_{data} = \frac{1}{N_{data}} \sum_{i=1}^{N_{data}} |u(t_i) - \hat{u}(t_i)|^2, \tag{3}$$

where $u(t_i)$ is the predictions of the Coagulo-Net whereas $\hat{u}(t_i)$ is the label data. It is noted that ideally, label data is considered to be the experimental data. However, in many real applications, the experimental measurements for specific coagulation factors may not be available. In this case, PINNs also allow utilization of the synthetic data or mixed experimental and synthetic data. Loss of ODE is the sum of the loss of initial conditions of the state variables ($\mathcal{L}_0$) and the residual loss of the ODEs of coagulation cascade models ($\mathcal{L}_r$) as expressed by

$$\mathcal{L}_{ODE} = w_0\mathcal{L}_0 + w_r\mathcal{L}_r \tag{4}$$

$$\mathcal{L}_0 = \frac{1}{N_0} \sum_{i=1}^{N_0} |u_i(t_0) - \hat{u}_i(t_0)|^2 \tag{5}$$

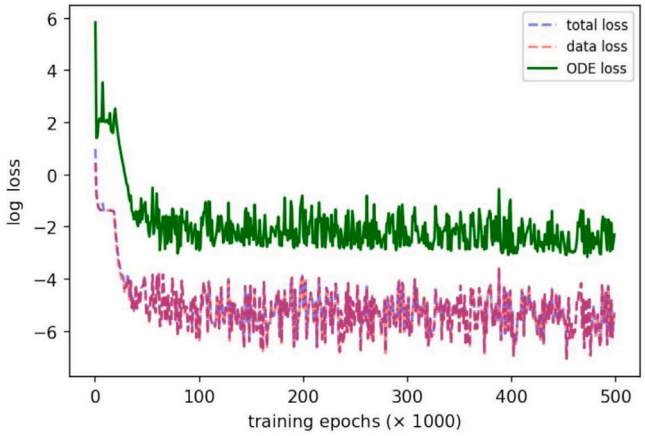

Fig. 2. The loss convergence process of Coagulo-Net. The total loss of Coagulo-Net equals to the sum of data loss and ODE loss. Coagulo-net is trained with 500,000 epochs.

$$\mathcal{L}_r = \frac{1}{N_{ODE}} \sum_{i=1}^{N_{ODE}} |f(t_i)|^2 \tag{6}$$

where N_0 represents the number of coagulation factors whose initial conditions are available. N_{ODE} denotes the number of equations involving the parameters needed to be estimated. $f(t)$ is defined to be given by the difference between the left-hand-side and right-hand-side of ODE; i.e., for the Eq. (1) in the ODE system,

$$f := \frac{du(t)}{dt} - g(u(t), t). \tag{7}$$

To infer the unknown model parameters, we will treat these parameters as trainable variables of the neural network such that these parameters can be inferred by fitting the predictions of Coagulo-Net with the targeted data during the training process of Coagulo-Net. We use the hyperbolic tangent function as the activation function, which is widely employed in many PINNs applications due to its smoothness. It is an essential feature for capturing the continuous nature of physical phenomena. To balance the contributions of loss of data and loss of ODE to the network training, we set the weights for data and ODE as 1.0 and 1e−5, respectively. We train the networks by 500,000 epochs with a learning rate of 0.001. As shown in Fig. 2, 500,000 training epochs are long enough for Coagulo-Net to converge. We use the Coagulo-net with the minimum total loss during 500,000 training epochs as the model for making predictions. We build Coagulo-Net using TensorFlow, an open-source software library for machine earning. Zarnitsina's model, involving 8 ODEs, requires 2212 s to complete training, while Susree's model, involving 34 ODEs, requires 4597 s.

3. Results

3.1. Baseline tests of Coagulo-Net

First, we perform a baseline test of the Coagulo-Net by providing all the data of coagulation concentration to the Coagulo-Net incorporated with Zarnitsina's model. All the kinetic parameters in the ODE system are adopted from the original work of Zarnitsina et al. (1996). The data of each species concentration contains 2000 points generated from the model, covering the temporal range from 0 to 100 min. Fig. 3 compares the dynamics of each species predicted by Coagulo-Net with the data generated by MATLAB, which is considered a reference. It is noted that for all the species, the curves generated by the Coagulo-Net and reference overlap, demonstrating the capability of the Coagulo-Net to accurately model the dynamics of each species by using the combination of data and ODEs.

Table 1
Identifiability analysis of Zarnitsina's model. The identifiability of the model parameters (lower panel) depends on the availability of the coagulation factors (upper panel). 9 cases (9 columns in the Table) with increased number of available state variables are examined. ✗ in the top panel represents unavailable while ✓ represents available. ✗ in the bottom panel represents unidentifiable while ✓ represents identifiable.

Test cases	Case	1	2	3	4	5	6	7	8	9
Data given	IX_a	✗	✓	✓	✓	✓	✓	✓	✓	✓
	X_a	✗	✗	✓	✓	✓	✓	✓	✓	✓
	II_a	✗	✗	✗	✓	✓	✓	✓	✓	✓
	II	✗	✗	✗	✗	✓	✓	✓	✓	✓
	$VIII_a$	✗	✗	✗	✗	✗	✓	✓	✓	✓
	V_a	✗	✗	✗	✗	✗	✗	✓	✓	✓
	APC	✗	✗	✗	✗	✗	✗	✗	✓	✓
	I_a	✗	✗	✗	✗	✗	✗	✗	✗	✓
Parameter identifiability	k_9	✗	✓	✓	✓	✓	✓	✓	✓	✓
	h_9	✗	✓	✓	✓	✓	✓	✓	✓	✓
	k_{10}	✗	✗	✓	✓	✓	✓	✓	✓	✓
	$\bar{k}_{10}$	✗	✗	✗	✗	✗	✓	✓	✓	✓
	h_{10}	✗	✗	✓	✓	✓	✓	✓	✓	✓
	k_2	✗	✗	✗	✓	✓	✓	✓	✓	✓
	$\bar{k}_2$	✗	✗	✗	✗	✗	✗	✓	✓	✓
	k_{2m}	✗	✗	✗	✓	✓	✓	✓	✓	✓
	$\bar{k}_{2m}$	✗	✗	✗	✓	✓	✓	✓	✓	✓
	h_2	✗	✗	✓	✓	✓	✓	✓	✓	✓
	k_8	✗	✗	✗	✗	✗	✓	✓	✓	✓
	h_8	✗	✗	✓	✓	✓	✓	✓	✓	✓
	k_a	✗	✗	✗	✗	✗	✗	✗	✓	✓
	k_5	✗	✗	✗	✗	✗	✗	✓	✓	✓
	h_5	✗	✗	✓	✓	✓	✓	✓	✓	✓
	k_{APC}	✗	✗	✗	✗	✗	✗	✗	✓	✓
	h_{APC}	✗	✗	✓	✓	✓	✓	✓	✓	✓
	k_1	✗	✗	✗	✗	✗	✗	✗	✗	✓
	$k_{5,10}$	✗	✗	✓	✓	✓	✓	✓	✓	✓
	$k_{8,9}$	✗	✗	✓	✓	✓	✓	✓	✓	✓
	$h_{5,10}$	✗	✗	✓	✓	✓	✓	✓	✓	✓
	$h_{8,9}$	✗	✗	✓	✓	✓	✓	✓	✓	✓

3.2. Solving inverse problems using Coagulo-Net

In this section, we will explore the capacity of the Coagulo-Net to infer model parameters based on the dynamics of the coagulation factors. This process is essential for developing new coagulation models where model parameters need to be identified based on available measurements of the coagulation factors. Before inferring the model parameters, we perform a structural identifiability analysis of Zarnitsina's model. Structural identifiability is a theoretical property of ODE systems that indicates whether the parameters of the examined system can be uniquely determined based on observational data. This analysis is an essential step before parameter estimation, ensuring that the parameters that need to be discovered in the ODEs through fitting the observational data are identifiable. As listed in Table 1, we will vary the availability of the eight state variables of Zarnitsina's model (top panel) and investigate the resultant identifiability of the twenty-two parameters involved in the ODEs (bottom panel). Specifically, we test 9 cases (9 columns in the Table 1) with an increased number of available state variables and report the resultant identifiability of the model parameters. The identifiability analysis is conducted using a Julia package named Structural Identifiability (Dong, Goodbrake, Harrington, & Pogudin, 2023). The result of this analysis is listed in Table 1, which shows that as more state variables become available, the number of identifiable model parameters will be increased. When all the data of state variables are available, all the parameters of Zarnitsina's model are identifiable.

After we acquire the knowledge of the identifiability of the model parameters, we assume that four parameters of the model parameters, namely ka, $k8$, $k5$, $h5$ are unknown as these four parameters were obtained by fitting the models with the measurement data in the

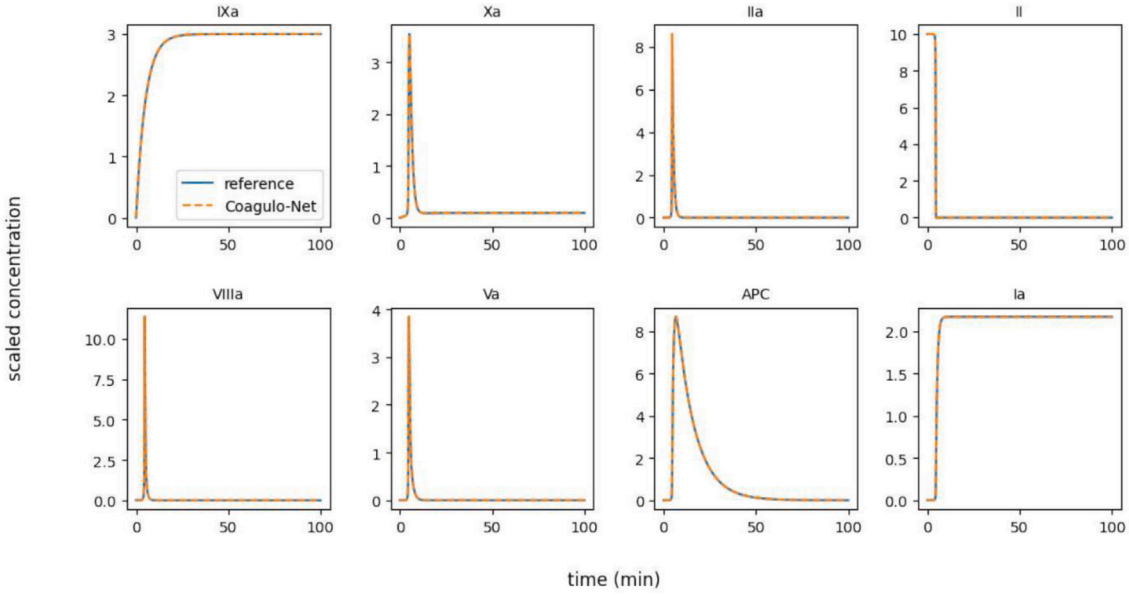

Fig. 3. Baseline test of Coagulo-Net' performance. Given data and ODE model with all model parameters, Coagulo-Net could output the dynamics of 8 coagulation factors that are consistent with the results of the original mathematical model.

Table 2
Inference of model parameters in Zarnitsina's model based on synthetic data.

Parameter	Inference	Reference	Relative error
ka	1.20130	1.2	0.00108
k8	9.44988e−06	1e−5	0.05501
k5	0.16998	0.17	0.00012
h5	0.30617	0.31	0.01235

original work of Zarnitsina et al. (1996). Given the data of the dynamics of eight species plus other model parameters adopted from prior work, we will infer these four unknown parameters and make predictions for concentrations over the temporal range as well. The predictions of the four unknown parameters and their reference values are listed in Table 2. Compared with the parameter values adopted from Zarnitsina's model, the relative errors of the model predictions range from 0.00012 to 0.05501. This extent of error will not affect the predictions of the dynamics for the coagulation factors, confirming the capability of Coagulo-Net to infer unknown model parameters in inverse problems. The predictions of the Coagulo-Net for the eight species are plotted in Fig. 4, which shows that the Coagulo-Net also could accurately simulate the dynamics of the eight species even with partially known parameters.

3.3. Predictions of Coagulo-Net based on sparse data

Researchers often encounter challenges in acquiring a large dataset of consistent and reliable measurements in biochemical experiments. Notably, the intricate process involved in coagulation cascade reactions limits the data generated within a reasonable timeframe. In this section, we aim to investigate the performance of the Coagulo-Net in solving the inverse problems with sparse data and explore to what extent data sparsity would affect the model's performance. The data points of sparse dataset are still distributed uniformly along the time-axis. Here, the sparsity is defined as the number of data points we omit divided by the number of data points we used in Sections 3.1 and 3.2. For example, compared with the dataset of 2000 points for describing the dynamics of each coagulation factor, a dataset with 1500 points has a sparsity of 25%. Following this definition, we examine the performance of Coagulo-Net using datasets with different sparsity of 0%, 25%, 50%, and 75%. The relative errors of the model predictions concerning the various extents of sparsity are summarized in Fig. 5, which shows that as data sparsity is elevated, the prediction error gradually increases. It is noted that Coagulo-Net could provide predictions with relatively low errors with 50% data sparsity, showcasing the robustness of Coagulo-Net towards data sparsity.

3.4. Predictions of Coagulo-Net based on noisy data

Measurement noise in biochemical experiments of blood coagulation is a critical concern due to the delicate and dynamic nature of the coagulation process. In such experiments, noise can originate from various sources, including biological variability among blood samples, instrumental inaccuracies, and environmental factors like temperature fluctuations. In this section, we aim to assess the performance of the Coagulo-Net in solving inverse problems using noisy data. To mimic data with different extents of noise, we generate Gaussian noise with varying scales of 1%, 5%, 10%, and 20% of the original dataset, add noise to original data, and then use these noisy data to infer the four unknown model parameters. The relative errors of the model predictions with respect to the different extents of noise are summarized in Fig. 6. It is noted that although the performance of the Coagulo-Net gradually deteriorates as the level of data noise increases, the prediction error is relatively low till the noise level reaches 20%. These results demonstrate the robustness of the Coagulo-Net in processing noisy data.

3.5. Performance of Coagulo-Net on a more sophisticated coagulation model

In the previous section, we systematically investigated the performance of Coagulo-Net on a relatively simple mathematical model of blood coagulation. In this section, we aim to assess Coagulo-Net's performance in solving a more complex model. Herein, we will incorporate Susree's model (Susree & Anand, 2017), which consists of 34

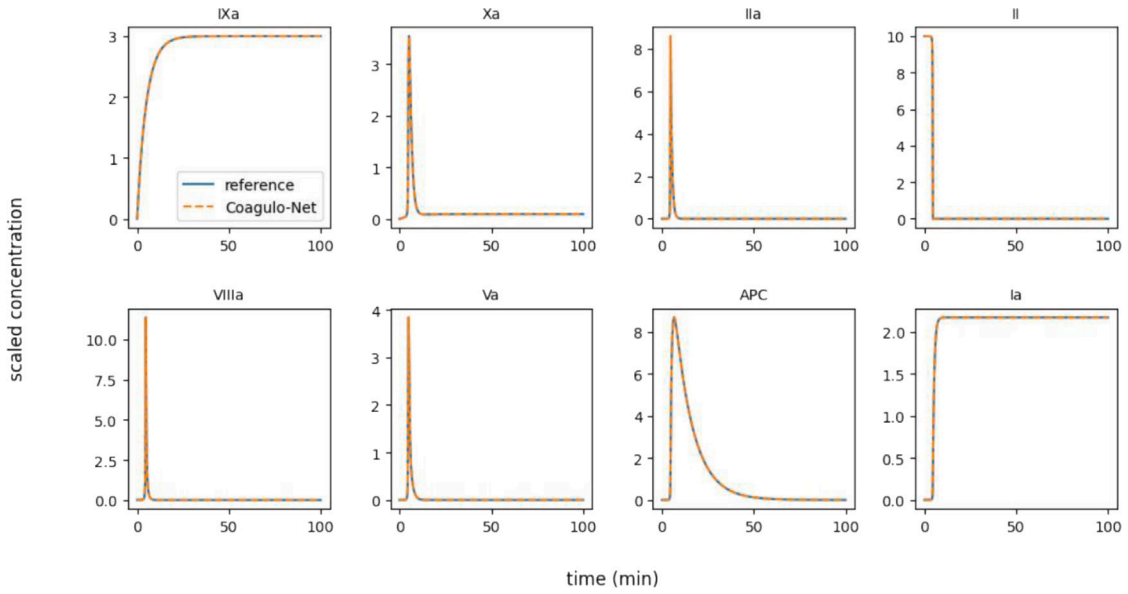

Fig. 4. Performance of solving an inverse problem using Coagulo-Net. Given data and ODE model with partial model parameters, Coagulo-Net could infer the unknown model parameters and output the dynamics of 8 coagulation factors that are consistent with the results of the original mathematical model.

Table 3
Inference of model parameters in Susree's model based on synthetic data.

Parameter	Inference	Reference	Relative error	Absolute error
(h_{10}^{TP+})	4.36377	4.381	0.00393	0.01723
(h_{10}^{TP-})	4.54392e−6	5.293e−8	84.84772	4.49099e−6
(h_2)	1.78848e−4	1.79e−4	0.00085	1.52e−6

Table 4
Inference of model parameters in Susree's model based on experiment data.

Parameter	Inference	Reference	Relative error	Absolute error
(h_{10}^{TP+})	4.36145	4.381	0.00446	0.01955
(h_{10}^{TP-})	1.96431e−4	5.293e−8	3710.14680	1.96378e−4
(h_2)	1.77839e−4	1.79e−4	0.00649	0.01161

ODEs (Susree & Anand, 2017). The detailed model formulation of Susree's model can be found in Appendix B. In the original work of Susree's model, three parameters, namely h_{10}^{TP+}, h_{10}^{TP-}, and h_2, were estimated by fitting the experimental data while the rest model parameters are inherited from prior models. Herein, we assume these parameters are unknown and attempt to infer these three parameters using Coagulo-net informed by coagulation factor dynamics over temporal range.

The results of parameter inference are summarized in Table 3. Compared with the parameter values reported from the original Susree's model, h_{10}^{TP+} and h_2's relative errors are very low, 0.00393 and 0.00085, respectively. As for h_{10}^{TP-}, its reference value is 5.293e−8, which is a very small value. Thus, we calculate its absolute error instead, and the absolute error of h_{10}^{TP-}'s inference is computed to be 4.49099e−6. Next, we put the parameters inferred by Coagulo-Net back into the ODEs MATLAB solver to solve the ODE system and plot the results in Fig. 7. These results show that the Coagulo-Net can successfully recover the parameters that result in the dynamics of coagulation factors that are consistent with the data generated from the original Susree's model. These results demonstrate that Coagulo-Net can accurately infer unknown parameters in more complex coagulation models.

We note that in the original work of Susree and Anand (2017), the three unknown model parameters are derived based on experimental measurements of the dynamics of the sum of IIa and IIa^m. As illustrated in Fig. 7, While the overall dynamic trend of the combined levels of IIa and IIa^m aligns with the experimental observations, there are significant differences observed between the model's predictions and the actual experimental results. Herein, we will use the experimental data to train the Coagulo-Net instead of the values generated from Susree's model. However, since only the experimental data of IIa and IIa^m are available, which is not sufficient to train the model and inform the dynamics of the rest 32 factors, we use Susree's model to generate synthetic data to supplement the training of Coagulo-Net. Specifically, the synthetic and real data will be treated differently during the training of the PINNs. First, we will compute two data loss terms for synthetic and real data, respectively, using different sets of time points because the real data is often more sparse than the synthetic data. Second, since experimental data is considered as high fidelity, we will give a higher weight factor for its loss term than those of synthetic data for training the Coagulo-Net. In the current study, we selected the weight factor for the loss attributed to experimental data as two times greater than that of synthetic data, but this could vary for different applications. The results of parameter inference utilizing the mixture of experimental and synthetic data are listed in Table 4. Compared with the original model parameter values reported in Susree's model, the inferred model parameters using mixed data are very close to the original Susree's models as the predictions of the original model are close to the experimental measurements. The resulting dynamics of IIa and IIa^m predicted by Coagulo-Net is shown in Fig. 8 where we observe that the predictions of Coagulo-Nets match very well with the experimental points in contrast to that of the Susree's model. These results demonstrate the critical feature of Coagulo-Net in fusing the mechanistic model with measurement data, which refines the predictions of mechanistic models.

4. Discussion and summary

Computational models of blood coagulation and clot formation play a pivotal role in advancing our understanding of the complex

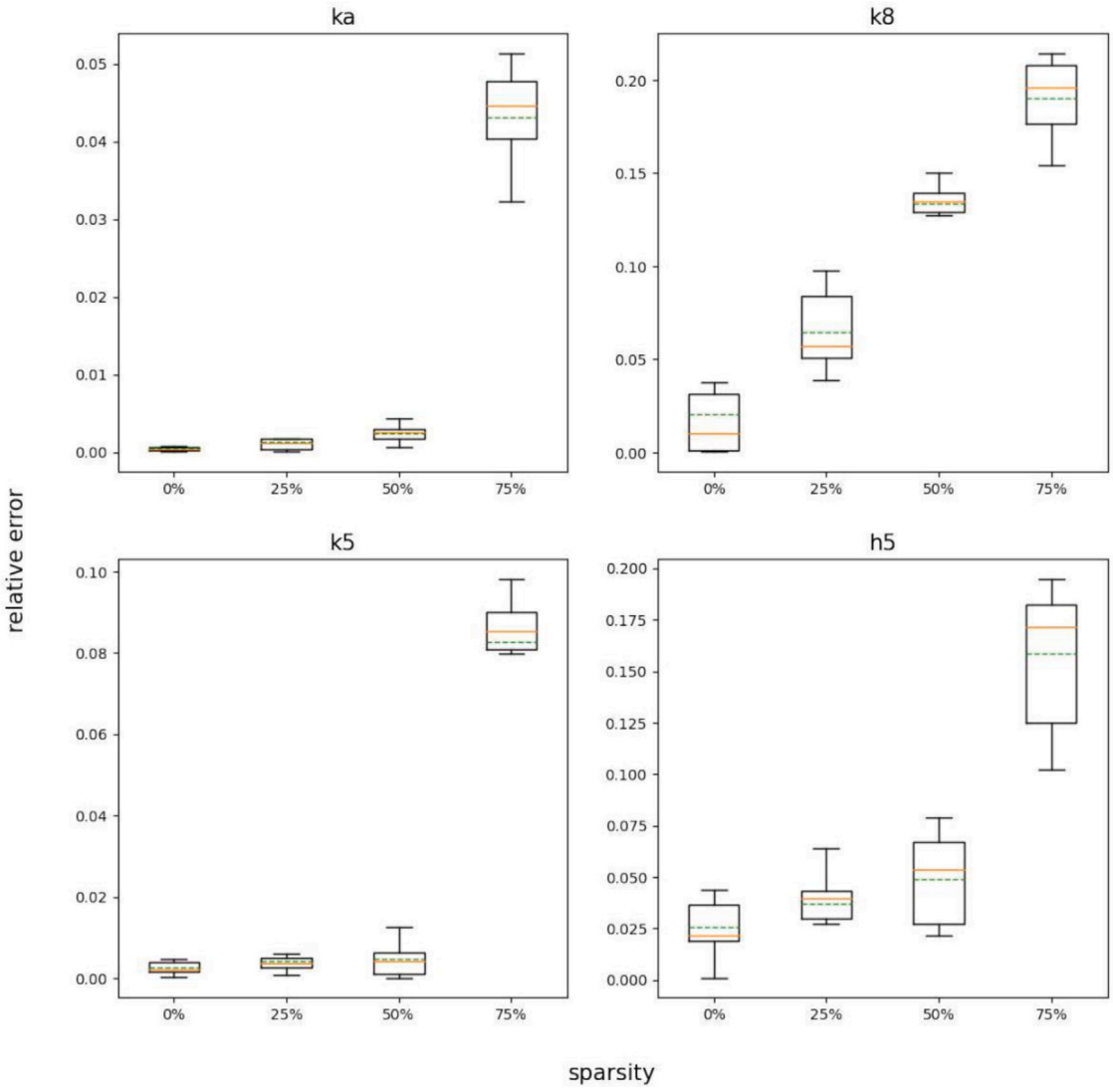

Fig. 5. Performance of Coagulo-Net based on sparse data. Prediction errors of Coagulo-Net for inferring four unknown parameters using data with different extents of sparsity. Each prediction is repeated ten times, and the mean and standard deviation of the prediction errors are plotted.

biological process involving hemostasis and thrombosis (Anand et al., 2022; Belyaev et al., 2018; Leiderman & Fogelson, 2014; Leiderman et al., 2021; Link et al., 2021; Neeves & Leiderman, 2016; Zhu et al., 2023). These models can simulate the complicated network of biochemical reactions involved in the enzymatic reactions in the intrinsic and extrinsic pathways leading to thrombin generation, simulation of platelet activation and aggregation, and clot formation and conversion of fibrinogen to fibrin that stabilizes the clot (Filla et al., 2024; Filla, Hou, Li, & Wang, 2023; Leiderman & Fogelson, 2011, 2013; Yazdani et al., 2021). The simulation results of the coagulation models have been used to decipher the pathophysiology of coagulation disorders like hemophilia and thrombosis, guide the design and testing of new anticoagulants or other therapeutic agents, facilitate the customized anticoagulant therapy based on the individual patient as well as enables prediction of clotting under various physiological conditions or in response to intervention. One of the critical challenges for developing computational models for simulating blood coagulation is to estimate the model parameters due to variability in biological data and limited experimental measurements. In this work, we introduce the Coagulo-Net, which is constructed based on PINN, one of the most popular models in the scientific machine learning area, to facilitate the estimation of the model parameters.

Since proposed in 2018, PINNs have been widely employed to solve PDEs and ODEs in science and engineering due to their capability to encode the underlying physical laws governed by either ODEs or PDEs into NNs (Cai et al., 2021; Chen, Li, & Zheng, 2024; Chen, Ye, Zhang, Li, & Zheng, 2023; Karniadakis et al., 2021; Linka et al., 2022; Lou, Meng, & Karniadakis, 2021; Lu et al., 2020; Lu, Meng, Mao, & Karniadakis, 2021; Meng, Li, Zhang, & Karniadakis, 2020; Raissi, Yazdani, & Karniadakis, 2020; Yang et al., 2021; Yu, Lu, Meng, & Karniadakis, 2022; Zhang, Zou, Kuhl, & Karniadakis, 2023; Zou & Karniadakis, 2023; Zou, Meng, & Karniadakis, 2023a, 2023b; Zou, Meng, Psaros, & Karniadakis, 2022). Combining NNs with physics-based models can help to infer unknown model parameters as constants or functions using limited data. This enables learning from "small data" as we explicitly utilize the constraints from the physical or biological laws, thereby rationalizing its application in developing the coagulation models. Our simulation results have shown that Coagulo-Nets could efficiently infer the unknown parameters in the coagulation models with different levels of complexity based on sparse data, data with noise, and experimental data, respectively, demonstrating the feasibility of

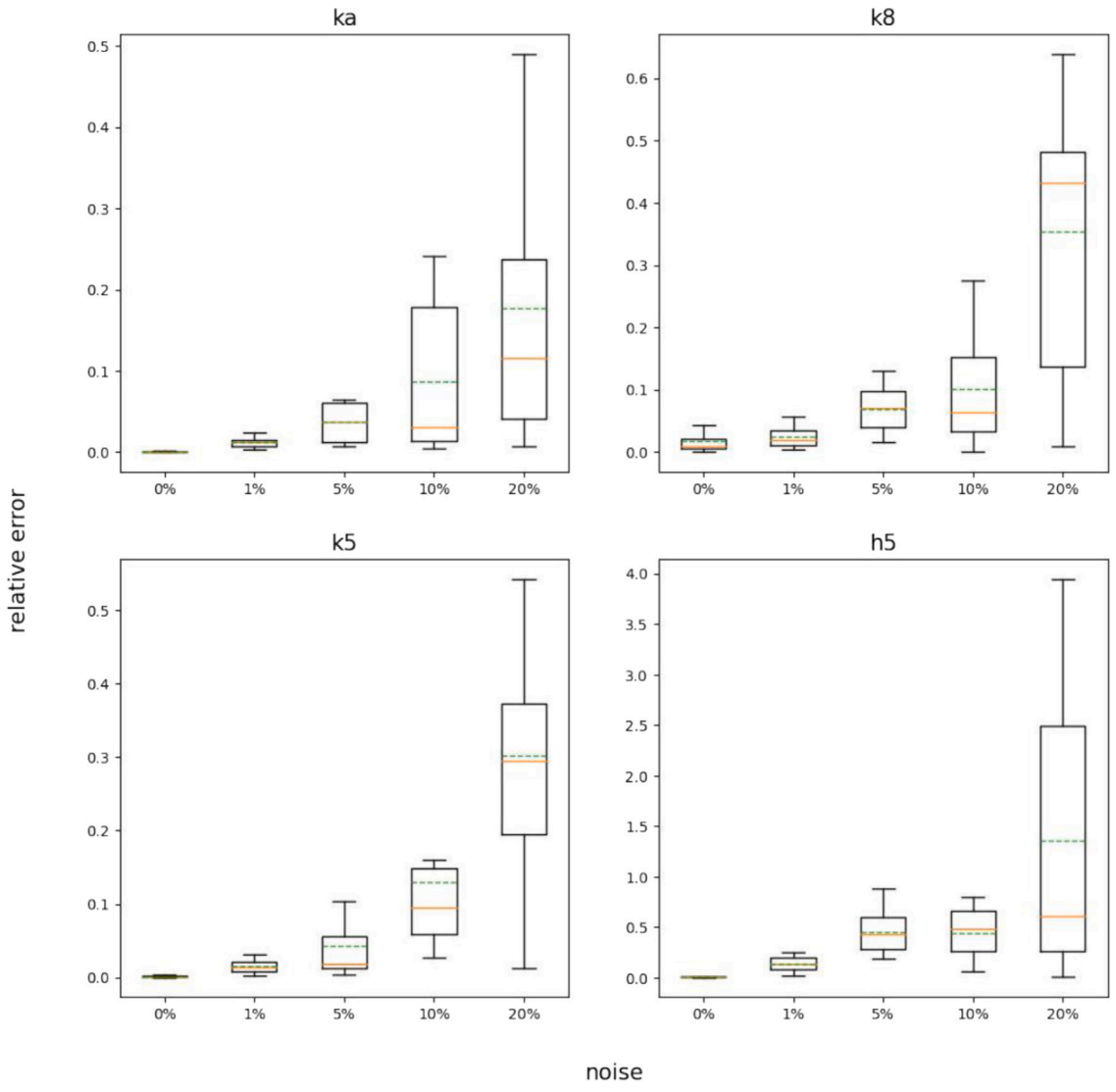

Fig. 6. Performance of Coagulo-Net based on noisy data. Prediction errors of Coagulo-Net for inferring four unknown parameters using data with different extents of noise. Each prediction is repeated ten times, and the mean and standard deviation of the prediction errors are plotted.

utilizing Coagulo-Net to refine the parameters in existing models and estimating parameters for new models.

In this study, we also employ the identifiability analysis to the coagulation model before inferring the unknown parameters using Coagulo-Net. While the motivation of the parameter identifiability analysis in the current study is to ensure that targeted unknown model parameters are identifiable before we perform inference for those parameters, it could have a larger impact on building a new coagulation model. In this context, identifiability analysis can be performed when the formulation of the new model is established to determine whether the model parameters involved are identifiable, which is essential for the model parameter fitting process. If some of the model parameters are analyzed to be unidentifiable, the formulation of the coagulation model needs to be revised to assure their identifiability.

We also note several limitations of Coagulo-Net: First, while we have successfully demonstrated the effectiveness of Coagulo-Net in established models, their accuracy and efficiency for developing new coagulation models remain to be explored. In particular, using more experimental data can introduce complexities and variations that may impact the model performances compared to the synthetic data. In addition, the suitability and practicality of Coagulo-Net are demonstrated by utilizing two ODE models in current research. Nevertheless, this does not preclude the potential application of Coagulo-Net to PDE models of blood coagulation (Bouchnita, 2017; Leiderman & Fogelson, 2011, 2013; Li, Deng, Li et al., 2022; Li, Deng, Sampani et al., 2022; Li et al., 2020; Panteleev et al., 2006; Yazdani et al., 2021, 2018; Yazdani, Li, Humphrey, & Karniadakis, 2017; Zarnitsina et al., 1996; Zheng, Yazdani, Li, Humphrey, & Karniadakis, 2020). As long as the development of a clot can be elucidated through mathematical models, it can be seamlessly integrated into the Coagulo-Net framework for parameter estimation. In addition, it is noted that the initial concentration of the coagulation factors is considered to be constant in the current study. However, they could vary for individual patients for a population study. In addition, the measurement data for calibrating the model parameters could be collected from different experimental settings and lab environments. These factors could result in uncertainty in estimating the model parameters (Psaros, Meng, Zou, Guo, & Karniadakis, 2023).

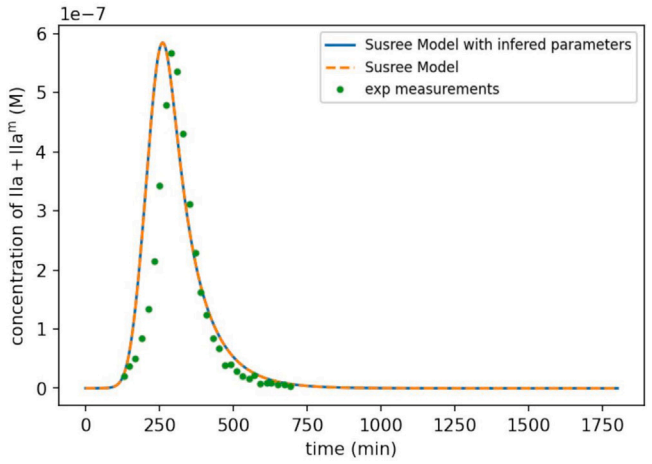

Fig. 7. The dynamics of the sum of IIa and IIa^m of the Susree model. Comparison of the dynamics of the sum of IIa and IIa^m among the experimental measurements, data generated using the original Susree model, and data generated using the Susree model with newly inferred parameters by Coagulo-Net.

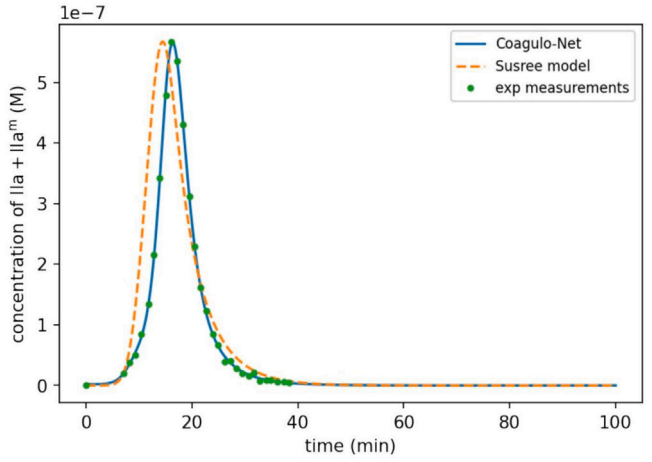

Fig. 8. The dynamics of the sum of IIa and IIa^m of the Susree model. Comparison of the dynamics of the sum of IIa and IIa^m among the experimental measurements, data generated using the original Susree model and predictions of Coagulo-Net.

To account for this uncertainty in the model prediction, we could adopt the framework of Bayesian physics-informed neural networks (B-PINNs) (Yang et al., 2021; Zou et al., 2022), which takes advantage of the function of PINNs in solving inverse problems and the capability of the Bayesian framework in quantification of the uncertainty for the model predictions.

In summary, this study introduces an innovative deep learning model into the computational modeling of blood coagulation by proposing Coagulo-Net, which could combine mathematical coagulation models with neural networks to infer the unknown model parameters more efficiently. Our simulation results demonstrate that Coagulo-Net may open a new avenue for refining existing coagulation models and facilitating the development of new models for physiological and pathological studies.

Nomenclature/notation

I: Fibrinogen
Ia: Fibrin
II: Prothrombin
IIa: Thrombin
TF: Tissue factor
IV: Calcium ions
V: Labile factor
VII: Proconvertin
VIII: Antihemophilic factor
IX: Christmas factor
X: Stuart-power factor
XII: Hageman factor
XIII: Fibrin stabilizing factor
(A:B): Coagulation factor complex
Aa: Activated form of coagulation factor 'A'
Am: Membrane-bound coagulation factor 'A'.
PC: Protein C.

Funding

This work was supported by National Institute of Health grants R21HL168507 and NSF SCH Award Number: 2406212. High-performance computing resources were provided by the Center for Computation and Visualization at Brown University and The Georgia Advanced Computing Resource Center (GACRC) at the University of Georgia.

CRediT authorship contribution statement

Ying Qian: Writing – original draft, Visualization, Validation, Software, Methodology, Investigation, Formal analysis, Data curation. **Ge Zhu:** Writing – original draft, Software, Methodology, Investigation, Data curation. **Zhen Zhang:** Methodology, Investigation, Formal analysis, Data curation. **Susree Modepalli:** Methodology, Investigation, Data curation. **Yihao Zheng:** Writing – original draft, Supervision. **Xiaoning Zheng:** Writing – original draft, Methodology, Conceptualization. **Galit Frydman:** Writing – original draft, Supervision, Conceptualization. **He Li:** Writing – review & editing, Writing – original draft, Supervision, Project administration, Methodology, Investigation, Funding acquisition, Data curation, Conceptualization.

Declaration of competing interest

The authors declare that they have no known competing financial interests or personal relationships that could have appeared to influence the work reported in this article.

Data availability

All relevant code and data are available from https://github.com/dpdclub/Coagulo-net.git.

Appendix A. Zarnitsina's model

Zarnitsina's model (Zarnitsina et al., 1996), which includes 8 ODEs, is listed below (8 ODE Model). c_1 to c_8 denotes IXa, Xa, IIa, II, VIIa, Va, APC and Ia respectively.

$$\frac{dc_1}{dt} = k_9 X Ia - h_9 c_1, \tag{A.1}$$

$$\frac{dc_2}{dt} = k_{10} c_1 + \bar{k}_{10} Z - h_{10} c_2, \tag{A.2}$$

$$\frac{dc_3}{dt} = k_2 \frac{c_2 c_4}{c_4 + k_{2m}} + \bar{k}_2 W \frac{c_4}{c_4 + \bar{k}_{2m}} - h_2 c_3, \tag{A.3}$$

$$\frac{dc_4}{dt} = -k_2 \frac{c_2 c_4}{c4 + k_{2m}} - \bar{k}_2 W \frac{c_4}{c_4 + \bar{k}_{2m}}, \tag{A.4}$$

$$\frac{dc_5}{dt} = k_8 c_3 - h_8 c_5 - k_a c_7 (c_5 + Z), \tag{A.5}$$

$$\frac{dc_6}{dt} = k_5 c_3 - h_5 c_6 - k_a c_7 (c_6 + W), \tag{A.6}$$

$$\frac{dc_7}{dt} = k_{APC} c_3 - h_{APC} c_7, \tag{A.7}$$

$$\frac{dc_8}{dt} = k_1 c_3. \tag{A.8}$$

where, $Z = k_{8,9} \frac{c_5 c_1}{h_{8,9} + k_a c_7}$, $W = k_{5,10} \frac{c_6 c_2}{h_{5,10} + k_a c_7}$.

The values for the kinetic parameters in the ODE system are adopted from Zarnitsina et al. (1996) and listed below. Besides, according to Zarnitsina's model, the initial concentrations of all active factors were set to zero. The initial concentration of XIa is 0.3 nM.

$k_9 = 20\ \text{min}^{-1}$
$h_9 = 0.2\ \text{min}^{-1}$
$k_8 = 0.00001\ \text{min}^{-1}$
$h_8 = 0.31\ \text{min}^{-1}$
$k_a = 1.2\ \text{nM}^{-1}\ \text{min}^{-1}$
$k_5 = 0.17\ \text{min}^{-1}$
$h_5 = 0.31\ \text{min}^{-1}$
$k_a = 1.2\ \text{nM}^{-1}\ \text{min}^{-1}$
$k_{10} = 0.003\ \text{min}^{-1}$
$\overline{k}_{10} = 500\ \text{min}^{-1}$
$h_{10} = 1\ \text{min}^{-1}$
$k_2 = 2.3\ \text{min}^{-1}, k_{2m} = 58\ \text{nM}$
$\overline{k}_2 = 2000\ \text{min}^{-1}, \overline{k}_{2m} = 210\ \text{nM}$
$h_2 = 1.3\ \text{min}^{-1}$
$k_{apc} = 0.0014\ \text{min}^{-1}$
$h_{apc} = 0.1\ \text{min}^{-1}$
$k_1 = 2.82\ \text{min}^{-1}$
$h_{11} = 0.2\ \text{min}^{-1}$
$k_{8,9} = 100\ \text{nM}^{-1}\ \text{min}^{-1}$
$h_{8,9} = 100\ \text{nM}^{-1}\ \text{min}^{-1}$
$k_{5,10} = 100\ \text{nM}^{-1}\ \text{min}^{-1}$
$h_{5,10} = 100\ \text{nM}^{-1}\ \text{min}^{-1}$

Appendix B. Susree's model

Susree's model (Susree & Anand, 2017), which includes 34 ODEs, are listed below.

$$G_{\text{TF}} = -k_{T7}^{+}[\text{TF}][\text{VII}] + k_{T7}^{-}[\text{TF} : \text{VII}] - k_{T7a}^{+}[\text{TF}][\text{VIIa}] + k_{T7a}^{-}[\text{TF} : \text{VIIa}]. \tag{B.1}$$

$$G_{\text{VII}} = -k_{T7}^{+}[\text{TF}][\text{VII}] + k_{T7}^{-}[\text{TF} : \text{VII}] - k_{TF7}[\text{TF} : \text{VIIa}][\text{VII}] - k_{10,7}[\text{Xa}][\text{VII}] - k_{2,7}[\text{IIa}][\text{VII}]. \tag{B.2}$$

$$G_{\text{TF:VII}} = k_{T7}^{+}[\text{TF}][\text{VII}] - k_{T7}^{-}\left[\text{VII}^{m}\right]. \tag{B.3}$$

$$G_{\text{VIIa}} = -k_{T7a}^{+}[\text{TF}][\text{VIIa}] + k_{T7a}^{-}[\text{TF} : \text{VIIa}] + k_{TF7}[\text{TF} : \text{VIIa}][\text{VII}] + k_{10,7}[\text{Xa}][\text{VII}] + k_{2,7}[\text{IIa}][\text{VII}]. \tag{B.4}$$

$$G_{\text{TF:VIIa}} = k_{T7a}^{+}[\text{TF}][\text{VIIa}] - k_{T7a}^{-}[\text{TF} : \text{VIIa}] - h_7^{TP}[\text{TFPI} : \text{Xa}][\text{TF} : \text{VIIa}] - h_7^{AT}[\text{ATIII}][\text{TF} : \text{VIIa}]. \tag{B.5}$$

$$G_{\text{IX}} = -\frac{k_9[\text{TF} : \text{VIIa}][\text{IX}]}{K_{9M} + [\text{IX}]} - k_9^{+} N_9[\text{AP}][\text{IX}] + k_9^{-}\left[\text{IX}^{m}\right]. \tag{B.6}$$

$$G_{\text{IXa}} = \frac{k_9[\text{TF} : \text{VIIa}][\text{IX}]}{K_{9M} + [\text{IX}]} - k_9^{+} N_9[\text{AP}][\text{IXa}] + k_9^{-}\left[\text{IXa}^{m}\right] - h_9[\text{IXa}][\text{ATIII}]. \tag{B.7}$$

$$G_{\text{IX}^{\text{m}}} = k_9^{+} N_9[\text{AP}][\text{IX}] - k_9^{-}\left[\text{IX}^{m}\right]. \tag{B.8}$$

$$G_{\text{IXa}^{\text{m}}} = -k_{TEN}^{+}\left[\text{VIIIa}^{m}\right]\left[\text{IXa}^{m}\right] + k_{TEN}^{-}\left[\text{VIIIa}^{m} : \text{IXa}^{m}\right] + k_9^{+} N_9[\text{AP}][\text{IXa}] - k_9^{-}\left[\text{IXa}^{m}\right]. \tag{B.9}$$

$$G_{\text{X}} = -\frac{k_{7,10}[\text{TF} : \text{VIIa}][\text{X}]}{K_{7,10M} + [\text{X}]} - k_{10}^{+} N_{10}[\text{AP}][\text{X}] + k_{10}^{-}\left[\text{X}^{m}\right]. \tag{B.10}$$

$$G_{\text{Xa}} = \frac{k_{7,10}[\text{TF} : \text{VIIa}][\text{X}]}{K_{7,10M} + [\text{X}]} - h_{10}^{TP+}[\text{TFPI}][\text{Xa}] + h_{10}^{TP-}[\text{Xa} : \text{TFPI}] - h_{10}^{AT}[\text{ATIII}][\text{Xa}] - k_{10}^{+} N_{10}[\text{AP}][\text{Xa}] + k_{10}^{-}\left[\text{Xa}^{\text{m}}\right]. \tag{B.11}$$

$$G_{\text{X}^{m}} = -\frac{k_{10}\left[\text{VIIIa}^{m} : \text{IXa}^{m}\right][\text{X}^{m}]}{K_{10M} + [\text{X}^{m}]} + k_{10}^{+} N_{10}[\text{AP}][\text{X}] - k_{10}^{-}\left[\text{X}^{m}\right]. \tag{B.12}$$

$$G_{\text{Xa}^{m}} = \frac{k_{10}\left[\text{VIIIa}^{m} : \text{IXa}^{m}\right][\text{X}^{m}]}{K_{10M} + [\text{X}^{m}]} - k_{\text{PRO}}^{+}\left[\text{Va}^{m}\right]\left[\text{Xa}^{m}\right] + k_{\text{PRO}}^{-}\left[\text{Va}^{m} : \text{Xa}^{m}\right] + k_{10}^{+} N_{10}[\text{AP}][\text{Xa}] - k_{10}^{-}\left[\text{Xa}^{\text{m}}\right]. \tag{B.13}$$

$$G_{\text{II}} = -k_{2t}[\text{Xa}][\text{II}] - k_2^{+} N_2[\text{AP}][\text{II}] + k_2^{-}\left[\text{II}^{m}\right]. \tag{B.14}$$

$$G_{\text{IIa}} = k_{2t}[\text{Xa}][\text{II}] - k_2^{+} N_2[\text{AP}][\text{IIa}] + k_2^{-}\left[\text{IIa}^{m}\right] - h_2\ [\text{ATIII}][\text{IIa}]. \tag{B.15}$$

$$G_{\text{II}^{m}} = -\frac{k_2\left[\text{Va}^{m} : \text{Xa}^{m}\right]\left[\text{II}^{m}\right]}{K_{2M} + \left[\text{II}^{m}\right]} + k_2^{+} N_2[\text{AP}][\text{II}] - k_2^{-}\left[\text{II}^{m}\right]. \tag{B.16}$$

$$G_{\text{IIa}^{m}} = \frac{k_2\left[\text{Va}^{m} : \text{Xa}^{m}\right]\left[\text{II}^{m}\right]}{K_{2M} + \left[\text{II}^{m}\right]} + k_2^{+} N_2[\text{AP}][\text{IIa}] - k_2^{-}\left[\text{IIa}^{m}\right]. \tag{B.17}$$

$$G_{\text{PL}} = -kpp[\text{PL}][\text{AP}] - \frac{kp2[\text{PL}][\text{IIa}]}{1 + [\text{IIa}]}. \tag{B.18}$$

$$G_{\text{AP}} = kpp[\text{PL}][\text{AP}] + \frac{kp2[PL][\text{IIa}]}{1 + [\text{IIa}]}. \tag{B.19}$$

$$G_{\text{VIII}} = -\frac{k_8[\text{IIa}][\text{VIII}]}{K_{8M} + [\text{VIII}]} - k_8^{+} N_8[\text{AP}][\text{VIII}] + k_8^{-}\left[\text{VIII}^{m}\right]. \tag{B.20}$$

$$G_{\text{VIIIa}} = \frac{k_8[\text{IIa}][\text{VIII}]}{K_{8M} + [\text{VIII}]} - k_8^{+} N_8[\text{AP}][\text{VIIIa}] + k_8^{-}\left[\text{VIIIa}^{m}\right] - h_8[\text{VIIIa}]. \tag{B.21}$$

$$G_{\text{VIII}^{m}} = -\frac{k_8^{m}\left[\text{IIa}^{m}\right]\left[\text{VIII}^{m}\right]}{K_{8M}^{m} + \left[\text{VIII}^{m}\right]} - \frac{k_{8t}^{m}\left[\text{Xa}^{m}\right]\left[\text{VIII}^{m}\right]}{K_{8tM}^{m} + \left[\text{VIII}^{m}\right]} + k_8^{+} N_8[\text{AP}][\text{VIII}] - k_8^{-}\left[\text{VIII}^{m}\right]. \tag{B.22}$$

$$G_{\text{VIIIa}^{m}} = \frac{k_8^{m}\left[\text{IIa}^{m}\right]\left[\text{VIII}^{m}\right]}{K_{8M}^{m} + \left[\text{VIII}^{m}\right]} + \frac{k_{8t}^{m}\left[\text{Xa}^{m}\right]\left[\text{VIII}^{m}\right]}{K_{8tM}^{m} + \left[\text{VIII}^{m}\right]} + k_8^{+} N_8[\text{AP}][\text{VIIIa}] - k_8^{-}\left[\text{VIIIa}^{m}\right] - k_{TEN}^{+}\left[\text{VIIIa}^{m}\right]\left[\text{IXa}^{m}\right] + k_{\text{TEN}}^{-}\left[\text{VIIIa}^{m} : \text{IXa}^{m}\right]. \tag{B.23}$$

$$G_{\text{VIIIa}^{m}:\text{IXa}^{m}} = k_{\text{TEN}}^{+}\left[\text{VIIIa}^{m}\right]\left[\text{IXa}^{m}\right] - k_{\text{TEN}}^{-}\left[\text{VIIIa}^{m} : \text{IXa}^{m}\right]. \tag{B.24}$$

$$G_{\text{V}} = -\frac{k_5[\text{IIa}][\text{V}]}{K_{5M} + [\text{V}]} - k_5^{+} N_5[\text{AP}][\text{V}] + k_5^{-}\left[\text{V}^{m}\right]. \tag{B.25}$$

Table 5
Initial concentrations of proteins and platelets in Susree's model as reported in Susree and Anand (2017).

Component	Normal conc. (nM)
TF	0.025
VII	10.0
VII^m	0.0
VIIa	0.1
$VIII^m$	0.0
IXa^m	0.0
IX^m	0.0
IXa	0.009
IX	90.0
Xa^m	0.0
X^m	0.0
Xa	0.017
X	170.0
IIa^m	0.0
II^m	0.0
IIa	0.140
II	1400.0
PL	10.0
AP	0.001
$VIIIa^m$	0.0
$VIII^m$	0.0
VIIIa	0.00007
VIII	0.7
IXa^m : $VIIIa^m$	0.0
Va^m	0.0
V^m	0.0
Va	0.002
V	20.0
Xa^m : Va^m	0.0
I	7000.0
Ia	0.70
TFPI	2.5
Xa:TFPI	0.0
ATIII	3400.0

$$G_{\mathrm{Va}} = \frac{k_5[\mathrm{IIa}][\mathrm{V}]}{K_{5M}+[\mathrm{V}]} - k_5^+ N_5[\mathrm{AP}][\mathrm{Va}] + k_5^- \left[\mathrm{Va}^m\right] - h_5[\mathrm{Va}]. \tag{B.26}$$

$$G_{\mathrm{V}^m} = -\frac{k_5^m[\mathrm{IIa}]\,[\mathrm{V}^m]}{K_{5M}^m+[\mathrm{V}^m]} - \frac{k_{5t}^m\left[\mathrm{Xa}^m\right][\mathrm{V}^m]}{K_{5tM}^m+[\mathrm{V}^m]} + k_5^+ N_5[\mathrm{AP}][\mathrm{V}] - k_5^-\left[\mathrm{V}^m\right]. \tag{B.27}$$

$$\begin{aligned} G_{\mathrm{Va}^m} = {} & \frac{k_5^m\,[\mathrm{IIa}^m]\,[\mathrm{V}^m]}{K_{5M}^m+[\mathrm{V}^m]} + \frac{k_{5t}^m\left[\mathrm{Xa}^m\right][\mathrm{V}^m]}{K_{5tM}^m+[\mathrm{V}^m]} - k_{\mathrm{PRO}}^+\left[\mathrm{Xa}^m\right]\left[\mathrm{Va}^m\right] \\ & + k_{\mathrm{PRO}}^-\left[\mathrm{Xa}^m : \mathrm{Va}^m\right] \\ & + k_5^+ N_5[\mathrm{AP}][\mathrm{Va}] - k_5^-\left[\mathrm{Va}^m\right]. \end{aligned} \tag{B.28}$$

$$G_{\mathrm{Xa}^m:\mathrm{Va}^m} = k_{\mathrm{PRO}}^+\left[\mathrm{Xa}^m\right]\left[\mathrm{Va}^m\right] - k_{\mathrm{PRO}}^-\left[\mathrm{Xa}^m : \mathrm{Va}^m\right]. \tag{B.29}$$

$$G_I = -\frac{k_f([\mathrm{IIa}])[\mathrm{I}]}{K_{fM}+[\mathrm{I}]}. \tag{B.30}$$

$$G_{Ia} = \frac{k_f([\mathrm{IIa}])[\mathrm{I}]}{K_{fM}+[\mathrm{I}]}. \tag{B.31}$$

$$G_{\mathrm{TFPI}} = -h_{10}^{TP+}[\mathrm{Xa}][\mathrm{TFPI}] + h_{10}^{TP-}[\mathrm{Xa} : \mathrm{TFPI}]. \tag{B.32}$$

$$\begin{aligned} G_{\mathrm{Xa:TFPI}} = {} & h_{10}^{TP+}[\mathrm{Xa}][\mathrm{TFPI}] - h_{10}^{TP-}[\mathrm{Xa} : \mathrm{TFPI}] \\ & - h_7^{TP}[\mathrm{TF} : \mathrm{VIIa}][\mathrm{Xa} : \mathrm{TFPI}]. \end{aligned} \tag{B.33}$$

$$G_{\mathrm{ATIII}} = -[\mathrm{ATIII}]\left(h_{10}^{\mathrm{AT}}[\mathrm{Xa}] + h_9[\mathrm{IXa}] + h_2[\mathrm{IIa}] + h_{T7}[\mathrm{TF} : \mathrm{VIIa}]\right). \tag{B.34}$$

There are dozens of kinetic parameters in Susree's model and their values are listed below.

$kpp = 0.3\ \mathrm{nM}^{-1}\ \mathrm{s}^{-1}$

$kp2 = 0.37\ \mathrm{s}^{-1}$

$k_{T7}^+ = 3.2 \times 10^{-03}\ \mathrm{nM}^{-1}\ \mathrm{s}^{-1}$

$k_{T7}^- = 3.1 \times 10^{-03}\ \mathrm{s}^{-1}$

$k_{T7a}^+ = 0.023\ \mathrm{nM}^{-1}\ \mathrm{s}^{-1}$

$k_{T7a}^- = 3.1 \times 10^{-03}\ \mathrm{s}^{-1}$

$k_{TF7} = 4.4 \times 10^{-04}\ \mathrm{nM}^{-1}\ \mathrm{s}^{-1}$

$k_{10,7} = 0.013\ \mathrm{nM}^{-1}\ \mathrm{s}^{-1}$

$k_{2,7} = 2.3 \times 10^{-05}\ \mathrm{nM}^{-1}\ \mathrm{s}^{-1}$

$h_7^{AT} = 4.5 \times 10^{-07}\ \mathrm{nM}^{-1}\ \mathrm{s}^{-1}$

$h_7^{TP} = 0.05\ \mathrm{nM}^{-1}\ \mathrm{s}^{-1}$

$k_9 = 0.26\ \mathrm{s}^{-1}$

$K_{9M} = 243.0\ \mathrm{nM}$

$h_9 = 2.223 \times 10^{-04}\ \mathrm{nM}^{-1}\ \mathrm{s}^{-1}$

$k_{7,10} = 1.15\ \mathrm{s}^{-1}$

$K_{7,10\ \mathrm{M}} = 450.0\ \mathrm{nM}$

$h_{10}^{AT} = 3.05 \times 10^{-06}\ \mathrm{nM}^{-1}\ \mathrm{s}^{-1}$

$h_{10}^{TP+} = 4.381\ \mathrm{nM}^{-1}\ \mathrm{s}^{-1}$

$h_{10}^{TP-} = 5.293 \times 10^{-08}\ \mathrm{nM}^{-1}\ \mathrm{s}^{-1}$

$k_{2t} = 7.5 \times 10^{-06}\ \mathrm{nM}^{-1}\ \mathrm{s}^{-1}$

$h_2 = 1.79 \times 10^{-04}\ \mathrm{nM}^{-1}\ \mathrm{s}^{-1}$

$k_8 = 0.9\ \mathrm{s}^{-1}$

$K_{8M} = 147.0\ \mathrm{nM}$

$h_8 = 0.0037\ \mathrm{s}^{-1}$

$k_5 = 0.233\ \mathrm{s}^{-1}$

$K_{5M} = 71.7\ \mathrm{nM}$

$h_5 = 0.0028\ \mathrm{s}^{-1}$

$k_f = 59.0\ \mathrm{s}^{-1}$

$K_{fM} = 3160.0\ \mathrm{nM}$

$k_9^+ = 0.01\ \mathrm{nM}^{-1}\ \mathrm{s}^{-1}$

$k_9^- = 0.0257\ \mathrm{s}^{-1}$

$k_{\mathrm{TEN}}^+ = 0.01\ \mathrm{nM}^{-1}\ \mathrm{s}^{-1}$

$k_{TEN}^- = 5.0 \times 10^{-03}\ \mathrm{s}^{-1}$

$k_{10}^+ = 0.029\ \mathrm{nM}^{-1}\ \mathrm{s}^{-1}$

$k_{10}^- = 3.3\ \mathrm{s}^{-1}$

$k_{10} = 8.33\ \mathrm{s}^{-1}$

$K_{10M} = 63.0\ \mathrm{nM}$

$k_{\mathrm{PRO}}^+ = 0.4\ \mathrm{nM}^{-1}\ \mathrm{s}^{-1}$

$k_{\mathrm{PRO}}^- = 0.2\ \mathrm{s}^{-1}$

$k_2^+ = 0.01\ \mathrm{nM}^{-1}\ \mathrm{s}^{-1}$

$k_2^- = 5.9\ \mathrm{s}^{-1}$

$k_2 = 22.4\ \mathrm{s}^{-1}$

$K_{2M} = 1060.0\ \mathrm{nM}$

$k_8^+ = 4.3 \times 10^{-03}\ \mathrm{nM}^{-1}\ \mathrm{s}^{-1}$

$k_8^- = 2.46 \times 10^{-03}\ \mathrm{s}^{-1}$

$k_8^m = 0.9\ \mathrm{s}^{-1}$

$K_{8M}^m = 200\ \mathrm{nM}$

$k_{8t}^m = 0.023\ \mathrm{s}^{-1}$

$K_{8tM}^m = 20.0\ \mathrm{nM}$

$k_5^+ = 0.057\ \mathrm{nM}^{-1}\ \mathrm{s}^{-1}$

$k_5^- = 0.17\ \mathrm{s}^{-1}$

$k_5^m = 0.23\ \mathrm{s}^{-1}$

$K_{5M}^m = 71.7\ \mathrm{nM}$

$k_{5t}^{m} = 0.046\ \mathrm{s}^{-1}$

$K_{5tM}^{m} = 10.4\ \mathrm{nM}$

The initial concentrations of proteins and platelets are listed in Table 5.

References

Anand, M., Panteleev, M. A., & Ataullakhanov, F. I. (2022). Computational models of hemostasis: Degrees of complexity. *Applications in Engineering Science*, Article 100103.

Bachman, F. (1987). Fibrinolysis. In *Clinical chemistry: an overview* (pp. 179–215). Springer.

Beltrami, Edward, & Jesty, Jolyon (1995). Mathematical analysis of activation thresholds in enzyme-catalyzed positive feedbacks: application to the feedbacks of blood coagulation. *Proceedings of the National Academy of Sciences*, *92*(19), 8744–8748.

Belyaev, A. V., Dunster, J. L., Gibbins, J. M., Panteleev, M. A., & Volpert, V. (2018). Modeling thrombosis in silico: Frontiers, challenges, unresolved problems and milestones. *Physics of Life Reviews*, *26*, 57–95.

Bouchnita, Anass (2017). *Mathematical modelling of blood coagulation and thrombus formation under flow in normal and pathological conditions* (Ph.D. thesis), Université de Lyon; École Mohammadia d'ingénieurs (Rabat, Maroc).

Bouchnita, Anass, Terekhov, Kirill, Nony, Patrice, Vassilevski, Yuri, & Volpert, Vitaly (2020). A mathematical model to quantify the effects of platelet count, shear rate, and injury size on the initiation of blood coagulation under venous flow conditions. *PLoS One*, *15*(7), Article e0235392.

Bouchnita, Anass, & Volpert, Vitaly (2019). A multiscale model of platelet-fibrin thrombus growth in the flow. *Computers & Fluids*, *184*, 10–20.

Bouchnita, Anass, Yadav, Kanishk, Llored, Jean-Pierre, Gurovich, Alvaro, & Volpert, Vitaly (2023). Thrombin generation thresholds for coagulation initiation under flow. *Axioms*, *12*(9), 873.

Bungay, Sharene D., Gentry, Patricia A., & Gentry, Rodney D. (2003). A mathematical model of lipid-mediated thrombin generation. *Mathematical Medicine and Biology*, *20*(1), 105–129.

Butenas, Saulius, van't Veer, Cornelis, & Mann, Kenneth G. (1999). "Normal" thrombin generation: Presented in part at the XVIth congress of the international society on thrombosis and haemostasis, june 6-12, 1997, Florence, Italy (abstr PS-1653), at the 15th international congress on thrombosis, october 16-21, 1998, Antalya, Turkey (abstr 234), and at the 40th annual meeting of the American society of hematology, december 4-8, 1998, Miami Beach, FL (abstr 151).. *Blood, the Journal of the American Society of Hematology*, *94*(7), 2169–2178.

Cai, Shengze, Li, He, Zheng, Fuyin, Kong, Fang, Dao, Ming, Karniadakis, George Em, et al. (2021). Artificial intelligence velocimetry and microaneurysm-on-a-chip for three-dimensional analysis of blood flow in physiology and disease. *Proceedings of the National Academy of Sciences*, *118*(13), Article e2100697118.

Cai, Shengze, Mao, Zhiping, Wang, Zhicheng, Yin, Minglang, & Karniadakis, George Em (2022). Physics-informed neural networks (PINNs) for fluid mechanics: A review. *Acta Mechanica Sinica*, 1–12.

Camerer, Eric, Huang, Wei, & Coughlin, Shaun R. (2000). Tissue factor-and factor X-dependent activation of protease-activated receptor 2 by factor VIIa. *Proceedings of the National Academy of Sciences*, *97*(10), 5255–5260.

Cash, Jeff R., & Karp, Alan H. (1990). A variable order runge-kutta method for initial value problems with rapidly varying right-hand sides. *ACM Transactions on Mathematical Software*, *16*(3), 201–222.

Chatterjee, Manash S, Denney, William S, Jing, Huiyan, & Diamond, Scott L (2010). Systems biology of coagulation initiation: kinetics of thrombin generation in resting and activated human blood. *PLoS Computational Biology*, *6*(9), Article e1000950.

Chatterjee, Manash S, Purvis, Jeremy E, Brass, Lawrence F, & Diamond, Scott L (2010). Pairwise agonist scanning predicts cellular signaling responses to combinatorial stimuli. *Nature Biotechnology*, *28*(7), 727–732.

Chen, Qijing, Li, He, & Zheng, Xiaoning (2024). A deep neural network for operator learning enhanced by attention and gating mechanisms for long-time forecasting of tumor growth. *Engineering with Computers*, 1–111.

Chen, Qijing, Ye, Qi, Zhang, Weiqi, Li, He, & Zheng, Xiaoning (2023). TGM-Nets: A deep learning framework for enhanced forecasting of tumor growth by integrating imaging and modeling. *Engineering Applications of Artificial Intelligence*, *126*, Article 106867.

Dahlbäck, Björn (2000). Blood coagulation. *The Lancet*, *355*(9215), 1627–1632.

Dashkevich, NM, Ovanesov, MV, Balandina, AN, Karamzin, SS, Shestakov, PI, Soshitova, NP, et al. (2012). Thrombin activity propagates in space during blood coagulation as an excitation wave. *Biophysical Journal*, *103*(10), 2233–2240.

De Ryck, Tim, Jagtap, Ameya D., & Mishra, Siddhartha (2024). Error estimates for physics-informed neural networks approximating the Navier–Stokes equations. *IMA Journal of Numerical Analysis*, *44*(1), 83–119.

Dong, Ruiwen, Goodbrake, Christian, Harrington, Heather A, & Pogudin, Gleb (2023). Differential elimination for dynamical models via projections with applications to structural identifiability. *SIAM Journal on Applied Algebra and Geometry*, *7*(1), 194–235.

Du, Pan, Zhu, Xiaozhi, & Wang, Jian-Xun (2022). Deep learning-based surrogate model for three-dimensional patient-specific computational fluid dynamics. *Physics of Fluids*, *34*(8), Article 081906.

Filla, Nicholas, Gu, Beikang, Hou, Jixin, Song, Kenan, Li, He, Liu, Ning, et al. (2024). Hyperelasticity of blood clots: Bridging the gap between microscopic and continuum scales. *Journal of the Mechanics and Physics of Solids*, Article 105750.

Filla, Nicholas, Hou, Jixin, Li, He, & Wang, Xianqiao (2023). A multiscale framework for modeling fibrin fiber networks: Theory development and validation. *Journal of the Mechanics and Physics of Solids*, *179*, Article 105392.

Fogelson, Aaron L., & Tania, Nessy (2005). Coagulation under flow: the influence of flow-mediated transport on the initiation and inhibition of coagulation. *Pathophysiology of Haemostasis and Thrombosis*, *34*(2–3), 91–108.

Furie, Bruce, & Furie, Barbara C. (2008). Mechanisms of thrombus formation. *New England Journal of Medicine*, *359*(9), 938–949.

Herrmann, FH, Koesling, M, Schröder, W, Altman, RJBR, Bonilla, R Jimenez, Lopaciuk, S, et al. (1997). Prevalence of factor v leiden mutation in various populations. *Genetic Epidemiology*, *14*(4), 403–411.

Hockin, Matthew F, Jones, Kenneth C, Everse, Stephen J, & Mann, Kenneth G (2002). A model for the stoichiometric regulation of blood coagulation. *Journal of Biological Chemistry*, *277*(21), 18322–18333.

Hoffman, Maureane, & Monroe III, Dougald M. (2001). A cell-based model of hemostasis. *Thrombosis and Haemostasis*, *85*(06), 958–965.

Jagtap, Ameya D., & Karniadakis, George Em (2020). Extended physics-informed neural networks (XPINNs): A generalized space-time domain decomposition based deep learning framework for nonlinear partial differential equations. *Communications in Computational Physics*, *28*(5).

Jagtap, Ameya D., Kawaguchi, Kenji, & Karniadakis, George Em (2020a). Locally adaptive activation functions with slope recovery for deep and physics-informed neural networks. *Proceedings of the Royal Society A*, *476*(2239), Article 20200334.

Jagtap, Ameya D., Kawaguchi, Kenji, & Karniadakis, George Em (2020b). Adaptive activation functions accelerate convergence in deep and physics-informed neural networks. *Journal of Computational Physics*, *404*, Article 109136.

Jagtap, Ameya D., Kharazmi, Ehsan, & Karniadakis, George Em (2020). Conservative physics-informed neural networks on discrete domains for conservation laws: Applications to forward and inverse problems. *Computer Methods in Applied Mechanics and Engineering*, *365*, Article 113028.

Jagtap, Ameya D, Mao, Zhiping, Adams, Nikolaus, & Karniadakis, George Em (2022). Physics-informed neural networks for inverse problems in supersonic flows. *Journal of Computational Physics*, *466*, Article 111402.

Karniadakis, George Em, Kevrekidis, Ioannis G, Lu, Lu, Perdikaris, Paris, Wang, Sifan, & Yang, Liu (2021). Physics-informed machine learning. *Nature Reviews Physics*, *3*(6), 422–440.

Kissas, Georgios, Yang, Yibo, Hwuang, Eileen, Witschey, Walter R, Detre, John A, & Perdikaris, Paris (2020). Machine learning in cardiovascular flows modeling: Predicting arterial blood pressure from non-invasive 4D flow MRI data using physics-informed neural networks. *Computer Methods in Applied Mechanics and Engineering*, *358*, Article 112623.

Kuharsky, Andrew L., & Fogelson, Aaron L. (2001). Surface-mediated control of blood coagulation: the role of binding site densities and platelet deposition. *Biophysical Journal*, *80*(3), 1050–1074.

Lei, Jing, Liu, Qibin, & Wang, Xueyao (2022). Physics-informed multi-fidelity learning-driven imaging method for electrical capacitance tomography. *Engineering Applications of Artificial Intelligence*, *116*, Article 105467.

Leiderman, Karin, & Fogelson, Aaron L. (2011). Grow with the flow: a spatial–temporal model of platelet deposition and blood coagulation under flow. *Mathematical Medicine and Biology: a Journal of the IMA*, *28*(1), 47–84.

Leiderman, Karin, & Fogelson, Aaron L. (2013). The influence of hindered transport on the development of platelet thrombi under flow. *Bulletin of Mathematical Biology*, *75*(8), 1255–1283.

Leiderman, Karin, & Fogelson, Aaron (2014). An overview of mathematical modeling of thrombus formation under flow. *Thrombosis Research*, *133*, S12–S14.

Leiderman, Karin, Sindi, Suzanne S, Monroe, Dougald M, Fogelson, Aaron L, & Neeves, Keith B (2021). The art and science of building a computational model to understand hemostasis. *Vol. 47*, In *Seminars in thrombosis and hemostasis* (pp. 129–138). Thieme Medical Publishers, Inc..

Li, He, Deng, Yixiang, Li, Zhen, Dorken Gallastegi, Ander, Mantzoros, Christos S, Frydman, Galit H, et al. (2022). Multiphysics and multiscale modeling of microthrombosis in COVID-19. *PLoS Computational Biology*, *18*(3), Article e1009892.

Li, He, Deng, Yixiang, Sampani, Konstantina, Cai, Shengze, Li, Zhen, Sun, Jennifer K, et al. (2022). Computational investigation of blood cell transport in retinal microaneurysms. *PLoS Computational Biology*, *18*(1), Article e1009728.

Li, He, Sampani, Konstantina, Zheng, Xiaoning, Papageorgiou, Dimitrios P, Yazdani, Alireza, Bernabeu, Miguel O, et al. (2020). Predictive modelling of thrombus formation in diabetic retinal microaneurysms. *Royal Society Open Science*, *7*(8), Article 201102.

Li, Shilin, Wang, Gang, Di, Yuelan, Wang, Liping, Wang, Haidou, & Zhou, Qingjun (2023). A physics-informed neural network framework to predict 3D temperature field without labeled data in process of laser metal deposition. *Engineering Applications of Artificial Intelligence*, *120*, Article 105908.

Li, G, Zhao, Y, Ma, W, Gao, Y, & Zhao, C (2024). Systems-level computational modeling in ischemic stroke: from cells to patients. *Frontiers in Physiology*, *15*, p.1394740.

Link, Kathryn G, Stobb, Michael T, Monroe, Dougald M, Fogelson, Aaron L, Neeves, Keith B, Sindi, Suzanne S, et al. (2021). Computationally driven discovery in coagulation. *Arteriosclerosis, Thrombosis, and Vascular Biology*, *41*(1), 79–86.

Linka, Kevin, Schäfer, Amelie, Meng, Xuhui, Zou, Zongren, Karniadakis, George Em, & Kuhl, Ellen (2022). Bayesian physics informed neural networks for real-world nonlinear dynamical systems. *Computer Methods in Applied Mechanics and Engineering*, *402*, Article 115346.

Lippi, Giuseppe, & Favaloro, Emmanuel J. (2020). D-dimer is associated with severity of coronavirus disease 2019: a pooled analysis. *Thrombosis and Haemostasis*, *120*(5), 876.

Lorenzo, Guillermo, Hormuth II, David A, Jarrett, Angela M, Lima, Ernesto ABF, Subramanian, Shashank, Biros, George, et al. (2022). Quantitative in vivo imaging to enable tumour forecasting and treatment optimization. In *Cancer, complexity, computation* (pp. 55–97). Springer.

Lou, Qin, Meng, Xuhui, & Karniadakis, George Em (2021). Physics-informed neural networks for solving forward and inverse flow problems via the Boltzmann-BGK formulation. *Journal of Computational Physics*, *447*, Article 110676.

Lu, Lu, Dao, Ming, Kumar, Punit, Ramamurty, Upadrasta, Karniadakis, George Em, & Suresh, Subra (2020). Extraction of mechanical properties of materials through deep learning from instrumented indentation. *Proceedings of the National Academy of Sciences*, *117*(13), 7052–7062.

Lu, Lu, Meng, Xuhui, Mao, Zhiping, & Karniadakis, George Em (2021). DeepXDE: A deep learning library for solving differential equations. *SIAM Review*, *63*(1), 208–228.

Mao, Zhiping, Jagtap, Ameya D., & Karniadakis, George Em (2020). Physics-informed neural networks for high-speed flows. *Computer Methods in Applied Mechanics and Engineering*, *360*, Article 112789.

Meng, Xuhui, Li, Zhen, Zhang, Dongkun, & Karniadakis, George Em (2020). PPINN: Parareal physics-informed neural network for time-dependent PDEs. *Computer Methods in Applied Mechanics and Engineering*, *370*, Article 113250.

Neeves, Keith B., & Leiderman, Karin (2016). Mathematical models of hemostasis. In *Trauma induced coagulopathy* (pp. 567–584). Springer.

Nguyen, Thi Nguyen Khoa, Dairay, Thibault, Meunier, Raphaël, & Mougeot, Mathilde (2022). Physics-informed neural networks for non-Newtonian fluid thermo-mechanical problems: An application to rubber calendering process. *Engineering Applications of Artificial Intelligence*, *114*, Article 105176.

Ouyang, Hanqing, Zhu, Zhicheng, Chen, Kuangqi, Tian, Beichen, Huang, Biao, & Hao, Jia (2023). Reconstruction of hydrofoil cavitation flow based on the chain-style physics-informed neural network. *Engineering Applications of Artificial Intelligence*, *119*, Article 105724.

Palta, Sanjeev, Saroa, Richa, & Palta, Anshu (2014). Overview of the coagulation system. *Indian Journal of Anaesthesia*, *58*(5), 515.

Panteleev, Mikhail A, Ovanesov, Mikhail V, Kireev, Dmitrii A, Shibeko, Aleksei M, Sinauridze, Elena I, Ananyeva, Natalya M, et al. (2006). Spatial propagation and localization of blood coagulation are regulated by intrinsic and protein C pathways, respectively. *Biophysical Journal*, *90*(5), 1489–1500.

Psaros, Apostolos F, Meng, Xuhui, Zou, Zongren, Guo, Ling, & Karniadakis, George Em (2023). Uncertainty quantification in scientific machine learning: Methods, metrics, and comparisons. *Journal of Computational Physics*, *477*, Article 111902.

Raissi, Maziar (2018). Deep hidden physics models: Deep learning of nonlinear partial differential equations. *Journal of Machine Learning Research*, *19*(1), 932–955.

Raissi, Maziar, Perdikaris, Paris, & Karniadakis, George E. (2019). Physics-informed neural networks: A deep learning framework for solving forward and inverse problems involving nonlinear partial differential equations. *Journal of Computational Physics*, *378*, 686–707.

Raissi, Maziar, Yazdani, Alireza, & Karniadakis, George Em (2020). Hidden fluid mechanics: Learning velocity and pressure fields from flow visualizations. *Science*, *367*(6481), 1026–1030.

Ren, Pu, Rao, Chengping, Sun, Hao, & Liu, Yang (2022). SeismicNet: Physics-informed neural networks for seismic wave modeling in semi-infinite domain. arXiv preprint arXiv:2210.14044.

Sahli Costabal, Francisco, Yang, Yibo, Perdikaris, Paris, Hurtado, Daniel E, & Kuhl, Ellen (2020). Physics-informed neural networks for cardiac activation mapping. *Frontiers in Physics*, *8*, 42.

Shukla, Khemraj, Jagtap, Ameya D, Blackshire, James L, Sparkman, Daniel, & Karniadakis, George Em (2021). A physics-informed neural network for quantifying the microstructural properties of polycrystalline nickel using ultrasound data: A promising approach for solving inverse problems. *IEEE Signal Processing Magazine*, *39*(1), 68–77.

Shukla, Khemraj, Jagtap, Ameya D., & Karniadakis, George Em (2021). Parallel physics-informed neural networks via domain decomposition. *Journal of Computational Physics*, *447*, Article 110683.

Susree, M., & Anand, M. (2017). A mathematical model for in vitro coagulation of blood: role of platelet count and inhibition. *Sādhanā*, *42*(3), 291–305.

Vandenbroucke, Jan P, Koster, Ted, Rosendaal, FR, Briët, E, Reitsma, PH, & Bertina, RM (1994). Increased risk of venous thrombosis in oral-contraceptive users who are carriers of factor V leiden mutation. *The Lancet*, *344*(8935), 1453–1457.

Yang, Liu, Meng, Xuhui, & Karniadakis, George Em (2021). B-PINNs: Bayesian physics-informed neural networks for forward and inverse PDE problems with noisy data. *Journal of Computational Physics*, *425*, Article 109913.

Yazdani, A., Deng, Y., Li, H., Javadi, E., Li, Z., Jamali, S., et al. (2021). Integrating blood cell mechanics, platelet adhesive dynamics and coagulation cascade for modelling thrombus formation in normal and diabetic blood. *Journal of the Royal Society Interface*, *18*(175), Article 20200834.

Yazdani, Alireza, Li, He, Bersi, Matthew R, Di Achille, Paolo, Insley, Joseph, Humphrey, Jay D, et al. (2018). Data-driven modeling of hemodynamics and its role on thrombus size and shape in aortic dissections. *Scientific Reports*, *8*(1), 1–18.

Yazdani, Alireza, Li, He, Humphrey, Jay D, & Karniadakis, George Em (2017). A general shear-dependent model for thrombus formation. *PLoS Computational Biology*, *13*(1), Article e1005291.

Yazdani, Alireza, Lu, Lu, Raissi, Maziar, & Karniadakis, George Em (2020). Systems biology informed deep learning for inferring parameters and hidden dynamics. *PLoS Computational Biology*, *16*(11), Article e1007575.

Yu, Jeremy, Lu, Lu, Meng, Xuhui, & Karniadakis, George Em (2022). Gradient-enhanced physics-informed neural networks for forward and inverse PDE problems. *Computer Methods in Applied Mechanics and Engineering*, *393*, Article 114823.

Zarnitsina, V. I., Pokhilko, A. V., & Ataullakhanov, F. I. (1996). A mathematical model for the spatio-temporal dynamics of intrinsic pathway of blood coagulation. I. The model description. *Thrombosis Research*, *84*(4), 225–236.

Zhang, Enrui, Dao, Ming, Karniadakis, George Em, & Suresh, Subra (2022). Analyses of internal structures and defects in materials using physics-informed neural networks. *Science Advances*, *8*(7), eabk0644.

Zhang, Zhen, Zou, Zongren, Kuhl, Ellen, & Karniadakis, George Em (2023). Discovering a reaction-diffusion model for alzheimer's disease by combining PINNs with symbolic regression. arXiv preprint arXiv:2307.08107.

Zheng, Xiaoning, Yazdani, Alireza, Li, He, Humphrey, Jay D, & Karniadakis, George E (2020). A three-dimensional phase-field model for multiscale modeling of thrombus biomechanics in blood vessels. *PLoS Computational Biology*, *16*(4), Article e1007709.

Zhu, Ge, Modepalli, Susree, Anand, Mohan, & Li, He (2023). Computational modeling of hypercoagulability in COVID-19. *Computer Methods in Biomechanics and Biomedical Engineering*, *26*(3), 338–349.

Zou, Zongren, & Karniadakis, George Em (2023). L-HYDRA: Multi-head physics-informed neural networks. arXiv preprint arXiv:2301.02152.

Zou, Zongren, Meng, Xuhui, & Karniadakis, George Em (2023a). Correcting model misspecification in physics-informed neural networks (PINNs). arXiv preprint arXiv:2310.10776.

Zou, Zongren, Meng, Xuhui, & Karniadakis, George Em (2023b). Uncertainty quantification for noisy inputs-outputs in physics-informed neural networks and neural operators. arXiv preprint arXiv:2311.11262.

Zou, Zongren, Meng, Xuhui, Psaros, Apostolos F, & Karniadakis, George Em (2022). NeuralUQ: A comprehensive library for uncertainty quantification in neural differential equations and operators. arXiv preprint arXiv:2208.11866.